

# Deep autoregressive models for the efficient variational simulation of many-body quantum systems

Or Sharir,<sup>1,\*</sup> Yoav Levine,<sup>1,†</sup> Noam Wies,<sup>1,‡</sup> Giuseppe Carleo,<sup>2,§</sup> and Amnon Shashua<sup>1,¶</sup>

<sup>1</sup>*The Hebrew University of Jerusalem, 9190401, Israel*

<sup>2</sup>*Center for Computational Quantum Physics, Flatiron Institute, 162 5th Avenue, New York, NY 10010, USA*

Artificial Neural Networks were recently shown to be an efficient representation of highly-entangled many-body quantum states. In practical applications, neural-network states inherit numerical schemes used in Variational Monte Carlo, most notably the use of Markov-Chain Monte-Carlo (MCMC) sampling to estimate quantum expectations. The local stochastic sampling in MCMC caps the potential advantages of neural networks in two ways: (i) Its intrinsic computational cost sets stringent practical limits on the width and depth of the networks, and therefore limits their expressive capacity; (ii) Its difficulty in generating precise and uncorrelated samples can result in estimations of observables that are very far from their true value. Inspired by the state-of-the-art generative models used in machine learning, we propose a specialized Neural Network architecture that supports efficient and exact sampling, completely circumventing the need for Markov Chain sampling. We demonstrate our approach for two-dimensional interacting spin models, showcasing the ability to obtain accurate results on larger system sizes than those currently accessible to neural-network quantum states.

*Introduction.*— The theoretical understanding and modeling of interacting many-body quantum matter represents an outstanding challenge since the early days of quantum mechanics. At the heart of several problems in condensed matter, chemistry, nuclear matter, and more lies the intrinsic difficulty of fully representing the many-body wave-function, in principle needed to exactly solve Schrödinger’s equation. These mainly fall into two categories: on one hand, there are states traditionally used in stochastic Variational Monte Carlo (VMC) calculations [1]. Chief example are Jastrow wave-functions [2], carrying high entanglement, but also with a limited variational freedom. On the other hand, more recently, tensor-network approaches have been put forward, based on non-stochastic variational optimization, and most chiefly on entanglement-limited variational wave-functions [3–6].

In an attempt to circumvent the limitations of the approaches above, neural-network-based architectures were proposed as variational wave functions [7]. Restricted Boltzmann machines (RBM), which represent relatively veteran machine learning constructs, were shown to be capable of representing volume-law entanglement scaling in 2D [8–11]. Recently, other neural-network architectures have been explored. Most notably, convolutional neural networks (ConvNets) – leading deep learning architectures that stand at the forefront of empirical successes in various Artificial Intelligence domains – have been applied to both bosonic [12] and frustrated spin systems [13].

Despite the provable theoretical advantage of ConvNet architectures [14], however, early numerical studies have

been limited to relatively shallow architectures, far from the very deep networks used in modern machine learning applications. This practical limitation is mostly due to two main factors. First, it is computationally expensive to obtain quantum expectation values over ConvNet states using stochastic sampling based on Markov Chain Monte Carlo (MCMC), as is it is customary in VMC applications. Second, there is an intrinsic optimization bottleneck to be faced when dealing with a large number of parameters. However, both limitations are routinely faced when learning deep autoregressive-models, recently introduced machine-learning techniques that have enabled previously intractable applications.

In this paper, we propose a pivotal shift in the use of Neural-network Quantum States (NQS) for many-body quantum systems, that markedly sets a discontinuity with traditionally adopted VMC methods. Inspired by the latest advances in generative machine learning models, we introduce variational states for which both the sampling and the optimization issues are substantially alleviated. Our model is composed of a ConvNet that allows direct, efficient, and i.i.d. sampling from the highly entangled wave function it represents. The network architecture draws upon successful autoregressive models for representing and sampling from probability distributions. Those are widely employed in the machine learning literature [15], and have been recently used for statistical mechanics applications [16], as well as density matrix reconstructions from experimental quantum systems [17]. We generalize these autoregressive models to treat complex-valued wave-functions, obtaining highly expressive architectures parametrizing an automatically normalized many-body quantum wave function.

*Neural Autoregressive Quantum States.*— We consider in the following a pure quantum system, constituted by  $N$  discrete degrees of freedom  $\mathbf{s} \equiv (s_1, \dots, s_N)$  (e.g. spins, occupation numbers, etc.) such that the wave-function amplitudes  $\Psi(\mathbf{s})$  fully specify its state. Here we follow

\* or.sharir@cs.huji.ac.il

† yoavlevine@cs.huji.ac.il

‡ noam.wies@cs.huji.ac.il

§ gcarleo@flatironinstitute.org

¶ shashua@cs.huji.ac.il

the approach introduced in [7], and represent  $\ln(\Psi(\mathbf{s}))$  as a feed-forward ANN, parametrized by a possibly large number of network connections. Given an arbitrary set of quantum numbers,  $\mathbf{s}$ , the output value computation of the corresponding NQS, known as its *forward pass*, can generally be described as a sequence of  $K$  matrix-vector multiplications separated by the applications of a non-linear element-wise *activation* function  $\sigma : \mathbb{C} \rightarrow \mathbb{C}$ . More formally, the unnormalized log amplitudes are given by

$$\ln(\Psi(\mathbf{s})) = W_K \sigma(W_{K-1} \sigma(\cdots \sigma(W_1 \mathbf{s}))), \quad (1)$$

where  $\mathcal{W} \equiv \{W_i \in \mathbb{C}^{r_i \times r_{i-1}}\}_{i=1}^K$ ,  $r_0 = N$ ,  $r_K = 1$ ,  $r_1, \dots, r_{K-1}$  are known as the *widths* of the network, and  $K$  as the *depth*. In practice, specialized variants of eq. 1 are commonly used, *e.g.* early applications have focused on shallow architectures ( $k = 1$ ) such as Restricted Boltzmann Machines, for which the activation function is typically taken to be  $\sigma(z) = \ln \cosh(z)$ . Other, deeper, choices are often advantageous, such as convolutional networks, in which most of the matrices are restricted to act on a subset of the quantum numbers, computing convolutions with small filters.

Given a NQS representation of a many-body quantum state, estimating physical observables  $\langle \Psi | \mathcal{O} | \Psi \rangle$  of a local operator  $\mathcal{O}$ , is in general analytically intractable, but can be realized numerically through a stochastic procedure, as done in VMC. Specifically,  $\langle \Psi | \mathcal{O} | \Psi \rangle = \langle \mathcal{O}^{\text{loc}} \rangle_{\mathcal{P}}$ , where  $\langle \dots \rangle_{\mathcal{P}}$  denote statistical expectation values over the Born probability density  $\mathcal{P}(\mathbf{s}) \equiv |\Psi(\mathbf{s})|^2$ , and  $\mathcal{O}^{\text{loc}} \equiv \sum_{\mathbf{s}'} \langle \mathbf{s} | \mathcal{O} | \mathbf{s}' \rangle \Psi(\mathbf{s}') / \Psi(\mathbf{s})$  is the corresponding statistical estimator. In the vast majority of VMC applications, including NQS so far, a MCMC algorithm is typically used to generate samples from  $\mathcal{P}(\mathbf{s})$ . While MCMC is a rather flexible technique, it comes with a large computational cost, especially for deep ANNs. Additionally, though MCMC asymptotically generates samples that are correctly distributed, in practice it can be plagued by very large autocorrelation times, and lack of ergodicity, that can severely affect the quality of the samples being generated.

In light of these limitations, we propose here a specialized network architecture that instead supports efficient and exact sampling. Our approach is an extension of Neural Autoregressive Density Estimators (NADE) [15] to quantum applications, resulting in what we dub *Neural Autoregressive Quantum States* (NAQS). To start with, first consider the task of representing a probability distribution with NADE models. These models build on the so-called autoregressive property, which entails a decomposition of the full probability distribution as a product of conditionals, *i.e.*  $P(s_1, \dots, s_N) = \prod_{i=1}^N p_i(s_i | s_{i-1}, \dots, s_1)$ . The power of these models comes from the observation that, for every  $i$ , the conditional probabilities  $p_i$  can be individually represented as an ANN receiving as input the variables  $s_1, \dots, s_{i-1}$  and outputting a vector  $\mathbf{v}_i \equiv (v_i(s^1), v_i(s^2) \dots v_i(s^M))$  representing the unnormalized probabilities for  $s_i$  to take one of the  $M$  possible discrete values  $s^j$ , conditioned on

given  $s_1, \dots, s_{i-1}$ . It is crucial that each output vector  $\mathbf{v}_i$  does not depend on the value of  $s_i$  or any of the variables appearing with a larger index,  $s_{i+1}, \dots, s_N$ , for a pre-chosen ordering. To ensure that each network outputs a valid conditional distribution, it is then sufficient to take the exponent of each entry and normalizing it according to the  $l_1$  norm, *i.e.*  $p_i(s_i | s_{i-1}, \dots, s_1) = \exp(v_i(s_i)) / \sum_{s'} |\exp(v_i(s'))|$ , also known as a *Softmax* operation.

Even though it is possible to use  $N$  separate networks for each of the  $N$  conditional probabilities, and each accepting a variable number of inputs, in practice it is more common to use a single ANN that accepts  $N$  inputs and outputs  $N$  probability vectors. In this case, the autoregressive property is enforced by masking the inputs  $s_i, \dots, s_N$  for the  $i$ 'th output vector, *i.e.* ensuring that the contributions of higher-ordered spins to the output of the network vanish. PixelCNN [18] is such an architecture, and is built as a sequence of *masked* convolutional layers, whose filters are restricted to having zeros at positions “ahead”. For example, in a one dimensional system, a filter of width  $R$ , where  $R$  is odd, would be constrained to have  $(w_1, \dots, w_{(R-1)/2}, 0, \dots, 0)$ , and thus the  $i$ th output of each layer depends uniquely on the indices at  $s_1, \dots, s_{i-1}$ .

A chief advantage of networks with the autoregressive property, is that directly drawing samples according to  $P(\mathbf{s})$  is conceptually straightforward. One can sample each  $s_i$  in sequence, according to its given conditional probability that depends just on the previously sampled  $(s_1, \dots, s_{i-1})$ . Carefully exploiting the intrinsic sparseness of the network weights, further leads to a very efficient algorithm for sampling [19]. Remarkably, the complexity of sampling a full string  $s_1 \dots s_N$  in a PixelCNN architecture can be reduced to the complexity of just a single forward pass.

Our NAQS model for representing wave-function is based on the same NADE principles so far described. Specifically, just as probability functions can be factorized into a product of conditional probabilities, we represent a normalized wave-function as a product of normalized *conditional* wave-functions, such that

$$\Psi(s_1, \dots, s_N) = \prod_{i=1}^N \psi_i(s_i | s_{i-1}, \dots, s_1), \quad (2)$$

where  $\psi_i(s_i | s_{i-1}, \dots, s_1)$  are such that, for any fixed  $(s_1, \dots, s_{i-1}) \in \{1, \dots, M\}^{i-1}$ , they satisfy the normalization condition  $\sum_{s'} |\psi_i(s' | s_{i-1}, \dots, s_1)|^2 = 1$ . If this condition holds, then a strong normalization condition for the full wave-function follows (see app. A for proof):

**Claim 1** *Let  $\Psi : [M]^N \rightarrow \mathbb{C}$  such that  $\Psi(s_1, \dots, s_N) = \prod_{i=1}^N \psi_i(s_i | s_{i-1}, \dots, s_1)$ , where  $\{\psi_i\}_{i=1}^N$  are normalized conditional wave-functions. Then,  $\Psi$  is normalized, *i.e.*,  $\sum_{s_1, \dots, s_N} |\Psi(s_1, \dots, s_N)|^2 = 1$ .*

As in the NADE case, we represent conditional wave-function with an ANN accepting

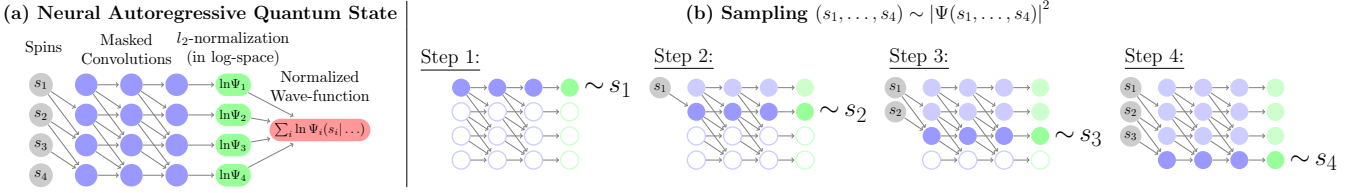


FIG. 1. A Neural Autoregressive Quantum State is a neural network that represents a normalized wave-function,  $\Psi(s_1, \dots, s_N)$ , by factoring it to a sequence of normalized *conditional* wave-functions, denoted by  $\Psi_i(s_i|s_{i-1}, \dots, s_1)$  for the  $i$ 'th particle, in a manner similar to that of Neural Autoregressive Density Estimator (see eq. 3). **(a)** Illustration of a deep 1D-convolutional NAQS model following the PixelCNN [18] architecture. Each column of nodes represent a layer in the network, starting with the input layer representing the  $N$ -particle configuration  $(s_1, \dots, s_N)$ . Each internal node in the graph is a complex vector computed according to its layer type. Namely, masked convolutions are limited to having local connectivity, where a node at the  $j$ 'th row is only connected to nodes with connections to  $s_i$  where  $i < j$ . All inputs to a node at the  $l$ 'th layer are multiplied by a matrix  $W^{(l)}$ , shared across all rows in the same layer, and followed by applying a non-linear element-wise function  $\sigma: \mathbb{C} \rightarrow \mathbb{C}$ . **(b)** Depicts the exact sampling algorithm for NAQS, where empty nodes represent unused nodes, and filled but faded nodes represent cached results from previous steps. The quantum number of each particle is generated sequentially, by computing its respective conditional wave-function, and sampling according to the squared magnitude. Notice that only a single row is processed at each step, and so sampling a complete configuration has the same runtime as a single forward pass.

$(s_1, \dots, s_{i-1})$  and outputting a complex vector  $\mathbf{v}_i \equiv (v_i(s^1), v_i(s^2) \dots v_i(s^M)) \in \mathbb{C}^M$  for each of the  $M$  possible values taken by the local quantum numbers  $s_i$ . To obtain a normalized conditional wave-function, we take its exponent and normalize it according to the  $l_2$ -norm, i.e.,  $\psi_i(s_i|s_{i-1}, \dots, s_1) = \exp(v_i(s_i)) / \sqrt{\sum_{s'} |\exp(v_i(s'))|^2}$ . Given this parametrization, the full wave-function log-amplitude  $\ln \Psi(s_1 \dots s_N)$  is easily obtained, once all the vectors  $\mathbf{v}_1, \dots, \mathbf{v}_N$  have been computed, as given by:

$$\ln \Psi(\mathbf{s}) = \sum_{i=1}^N \left( v_i(s_i) - \frac{1}{2} \ln \sum_{s'} |\exp(v_i(s'))|^2 \right). \quad (3)$$

As in the probabilistic autoregressive model, we can represent the entire NAQS by a single neural network outputting  $N$  complex vectors, as illustrated in Fig. 1a. Though our proposed architecture can work with either complex- or real-parameters, we have found that using the latter work better, where we output two real values, a log magnitude and phase, for every complex conditional log-amplitude.

Moreover, there is a special relationship between a NAQS and its induced Born probability, since  $|\Psi(s_1, \dots, s_N)|^2 = \prod_{i=1}^N |\psi_i(s_i|s_{i-1}, \dots, s_1)|^2$ , implying that  $|\psi_i(s)|^2$  is a valid conditional probability. Thus, the induced Born probability of a NAQS has the exact same structure of a NADE model. Specifically, taking the squared magnitude of its output vectors, i.e.,  $\bar{v}_i = |\hat{v}_i|^2$ , transform NAQS into a standard NADE representation of this distribution, which importantly includes its efficient and exact sampling method. In contrast to standard MCMC sampling employed for correlated wave-functions, NAQS thus allows for direct, efficient sampling with the computational complexity of a single forward pass, as depicted in Fig. 1b.

*Optimization.*— The NAQS representation of many-body wave functions can be used in practice for sev-

eral applications. These include for example ground-state search [7], quantum-state tomography [20], dynamics [7], and quantum circuits simulation [21]. Here we more specifically focus on the task of finding the ground state of a given Hamiltonian  $\mathcal{H}$ . In this context, we denote by  $\Psi_{\mathcal{W}}$  the wave-function represented by a NAQS of a fixed architecture that is parameterized by  $\mathcal{W}$ , and we wish to find  $\mathcal{W}$  values that minimize the energy, i.e.,  $\mathcal{W}^* = \text{argmin}_{\mathcal{W}} E(\mathcal{W})$ , where

$$E(\mathcal{W}) \equiv \langle \Psi_{\mathcal{W}} | \mathcal{H} | \Psi_{\mathcal{W}} \rangle = \mathbb{E}_{\mathbf{s} \sim |\Psi_{\mathcal{W}}|^2} [E_{\text{loc}}(\mathbf{s}; \mathcal{W})] \quad (4)$$

$$E_{\text{loc}}(\mathbf{s}; \mathcal{W}) \equiv \sum_{s'} \mathcal{H}_{\mathbf{s}, s'} \frac{\Psi_{\mathcal{W}}(s')}{\Psi_{\mathcal{W}}(\mathbf{s})}, \quad (5)$$

and  $\mathcal{H}$  is usually a highly sparse matrix, and so computing  $E_{\text{loc}}$  for a given sample takes at most  $O(N)$  forward passes.

The common approach for solving the optimization problem above with an NQS is to estimate the gradient of  $E(\mathcal{W})$  with respect to  $\mathcal{W}$ , and use variants of gradient descent to find the minimizer of  $E(\mathcal{W})$ . Estimating the gradient can be done by first employing a variant of the log-derivative trick, i.e.,

$$\frac{\partial E}{\partial \mathcal{W}} = \mathbb{E}_{\mathbf{s} \sim |\Psi_{\mathcal{W}}|^2} \left[ 2 \text{Re} \left( (E_{\text{loc}}(\mathbf{s})^* - E^*) \frac{\partial \ln \Psi_{\mathcal{W}}}{\partial \mathcal{W}} \right) \right]. \quad (6)$$

Now, while we can efficiently compute the log derivative of  $\Psi_{\mathcal{W}}$ , exactly computing the expected value is intractable, but we can still approximate it by computing its value over a finite batch of samples  $\{\mathbf{s}^{(i)}\}_{i=1}^B$ . The quality of this approximation depends on the batch size,  $B$ , but also on the degree of correlations between the individual samples. The advantages of our direct sampling method supported by NAQS over MCMC are twofold in this context: (i) Faster sampling: each individual sample can be generated with fewer network passes, and generating a batch of samples is embarrassingly parallel, as

$\Gamma$	NAQS Energy	QMC Energy	NAQS $\langle  \sigma_z  \rangle$	QMC $\langle  \sigma_z  \rangle$
2.0J	-2.4096022(2)	-2.40960(3)	0.78326(2)	0.78277(38)
2.5J	-2.7476550(5)	-2.74760(3)	0.57572(3)	0.57566(63)
3.0J	-3.1739005(5)	-3.17388(4)	0.16179(4)	0.16207(54)
3.5J	-3.6424799(3)	-3.64243(4)	0.11094(3)	0.11011(30)
4.0J	-4.1217979(2)	-4.12178(4)	0.09725(2)	0.09728(24)

TABLE I. Estimates of the ground state energies of the transverse-field Ising model for different values of  $\Gamma$  on a  $12 \times 12$  lattice, and the corresponding estimates of  $\langle \sigma_z \rangle$ , as obtained by either NAQS or QMC.

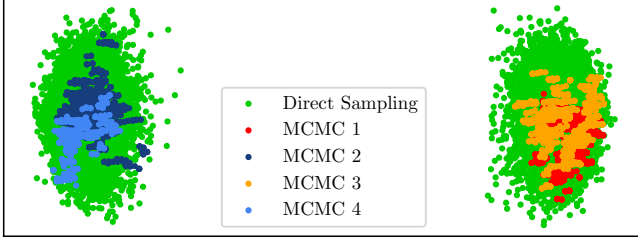


FIG. 2. An illustration of the two modes of the ground state, by taking the first two principal components of the generated samples. The green points correspond to our direct sampling method, and the other colors represent different MCMC chains. The plot was generated by training a NAQS on the transverse-field Ising model with  $\Gamma = 2J$ , below the critical value, on a  $12 \times 12$  lattice until convergence to the ground state, and then sampling from the trained NAQS using either our direct sampling method, or 4 separate MCMC samplers.

opposed to the sequential nature of MCMC; (ii) Faster convergence: because the generated samples are exact and i.i.d., and so result in more accurate estimates of the gradient at each step.

*Experiments.*— As a first benchmark for our approach, we consider a case where MCMC sampling can be strongly biased. A paradigmatic quantum system exhibiting this issue is found in the ferromagnetic phase of the transverse field Ising model. The Hamiltonian for this model is given by:

$$H = -J \sum_{\langle i,j \rangle} \sigma_z^i \sigma_z^j - \Gamma \sum_i \sigma_x^i, \quad (7)$$

where the summation runs over pairs of lattice edges. Here we study the case of a 2D square lattice with open boundary conditions, and for varying strengths of the transverse field. The system is in a ferromagnetic phase when the transverse magnetic field  $\Gamma$  is weak with respect to the coupling constant, and specifically in 2D when  $\Gamma < \Gamma_c \simeq 3.044J$  [22].

In order to verify the correctness of the model proposed in section 2, we begin by comparing the ground state energy and system magnetization obtained for a  $12 \times 12$  system with those obtained by an unbiased quantum Monte Carlo (QMC) simulation. We employ a NAQS model following the PixelCNN architecture, using the ADAM [23]

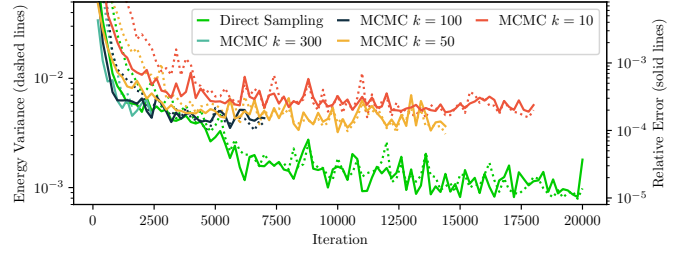


FIG. 3. Comparing the effects of the sampling method, either MCMC or direct sampling, on the training procedure for the transverse-field Ising model with  $\Gamma = 3J$ , close to the critical value, on a large ( $21 \times 21$ ) lattice. When using MCMC, samples are taken every  $k \in \{10, 50, 100, 300\}$  steps in the chain, where increasing  $k$  reduces the correlation between samples at the expense of increased computational cost. The solid lines shows the relative error to the minimal energy found for this system in our experiments, and dashed lines shows the energy variance. Since MCMC takes a considerable time to complete just a single iteration, we have restricted the training to maximum of 100 hours.

SGD variant with the gradient estimator of eq. 6. Additional technical details are listed in app. B. Table I shows that our model achieves very high accuracy for both magnetization and energy densities for different transverse field values across the phase diagram: when the system is in the ferromagnetic phase, the normal phase, and near the phase transition.

In order to quantify the behavior of our model in a region of broken symmetry, we consider the case of a transverse-field deep in the ferromagnetic region, namely  $\Gamma = 2J$ . The PCA visualization in Fig. 2 shows that for this value of  $\Gamma$  the MCMC chains initialized at one of the oriented states composing the ground state are stuck at that specific orientation and cannot come around to sampling spin configurations that correspond to the opposite orientation. In contrast, spin configurations sampled directly from the distribution by using our proposed technique include equally probable configurations from both orientations. The ergodicity breaking in local MCMC is also directly quantifiable by the expectation value of the total magnetization  $m = \langle \sum_i \sigma_i^z \rangle$ , for which we expect  $m = 0$  on any finite lattice. Indeed, the i.i.d. sampling enabled by our model correctly explores the two relevant ferromagnetic states (in agreement to the visualization of Fig. 2) and reaches a value close to a total zero magnetization, in stark contrast with MCMC estimation that effectively computes  $\langle |\sigma_z| \rangle \approx 0.78$  rather than  $m$ . As expected, directly estimating  $\langle |\sigma_z| \rangle$  with our sampling method correctly recovers it to a high precision, see Table I.

The limitation of the MCMC procedure in providing independent samples is not only conceptually relevant, but it can also have consequences on the quality of the resulting ground-state approximations. In Fig. 3, we show the training procedure for the transverse-field  $\Gamma = 3J$ , close to the critical value on a larger system ( $21 \times 21$ ).



	PEPS	NAQS	QMC
Energy	-0.628601(2)	-0.628627(1)	-0.628656(2)

TABLE II. Ground state energies for the antiferromagnetic Heisenberg model with open boundary conditions, as obtained by a state-of-the-art PEPS model [24], our NAQS model, and the exact QMC estimation, as reported in Liu *et al.* [24].

The same NAQS architecture was trained once with the i.i.d. sampling procedure and once with MCMC chains of varying lengths. The optimization advantage obtained when relying on independent samples clearly emerges from those figures – this procedure is much quicker and results in a significantly more accurate ground state energy and lower energy variance  $\langle H^2 \rangle - \langle H \rangle^2$ .

As a further benchmark, we also apply our method to a more complex system, the two-dimensional antiferromagnetic Heisenberg model with open boundary conditions, whose Hamiltonian is given by:

$$H = \sum_{\langle i,j \rangle} \sigma_x^i \sigma_x^j + \sigma_y^i \sigma_y^j + \sigma_z^i \sigma_z^j. \quad (8)$$

We evaluate our approach by comparing the ground state energy obtained for a  $10 \times 10$  system with those obtained by QMC simulations, as well as other variational methods. We find that NAQS meaningfully improve upon the accuracy of the best known variational methods for this problem. Namely, a relative error of  $8.7 \times 10^{-5} \pm 0.6 \times 10^{-5}$  was reported in Liu *et al.* [24] using a PEPS model, whereas with our approach we were able to obtain  $4.5 \times 10^{-5} \pm 0.4 \times 10^{-5}$ . See table II for exact results. Moreover, though they are not directly comparable, it is noteworthy that the relative error of the ground state energy with *periodic* boundary conditions obtained by NQS with MCMC sampling is significantly less accurate than ours (Carleo and Troyer [25], Choo *et al.* [26] report relative error greater than  $2 \times 10^{-4}$ ).

*Discussion.* – In this work, we have shown a scheme to facilitate the practical employment of contemporary deep learning architectures to the modeling of many-body quantum systems. This constitutes a striking improvement over currently used RBM methods that are limited to only hundreds of parameters, and very shallow networks. A further practical advantage we gain is the ability to make use of the substantial body of knowledge regarding optimization of these architectures that is accumulating in the deep learning literature. We empirically demonstrate that by employing common deep learning optimization methods such as stochastic gradient descent (SGD), our direct sampling approach allows us to train very large convolutional networks (depth 20, input size  $21 \times 21$ ,  $\sim 1$  million parameters). Our presented experiments demonstrate that even for relatively simple systems MCMC sampling can fail, while the i.i.d. sampling enabled by our model succeeds. Relying on the theoretically promising results regarding convolutional networks’ capabilities in representing highly entangled systems [14],

we view the enabling of their optimization as an integral step in reaching currently unattainable insight on a vast variety of quantum many body phenomena.

## ACKNOWLEDGMENTS

This work is supported by ISF Center grant 1790/12 and by the European Research Council (TheoryDL project). Yoav Levine is supported by the Adams Fellowship Program of the Israel Academy of Sciences and Humanities. QMC simulations for the 2D Transverse-Field Ising Model have been performed using the open-source ALPS Library [27].

## Appendix A: Proof of Claim 1

The proof follows an induction argument. For  $N = 1$ , it holds that  $\Psi(s_1) \equiv \Psi_1(s_1)$ , and so  $\Psi$  is normalized because  $\Psi_1$  is normalized with respect to  $s_1$ . Assume the claim holds for  $N = k$ , then for  $N = k + 1$  we first define  $\tilde{\Psi}(s_1, \dots, s_k) \equiv \prod_{i=1}^k \Psi_i(s_i | s_{i-1}, \dots, s_1)$ , and so

$$\begin{aligned} & \sum_{s_1, \dots, s_{k+1}} |\Psi(s_1, \dots, s_{k+1})|^2 \\ &= \sum_{s_1, \dots, s_{k+1}} \prod_{i=1}^{k+1} |\Psi_i(s_i | s_{i-1}, \dots, s_1)|^2 \\ &= \sum_{s_1, \dots, s_k} \left( \prod_{i=1}^k |\Psi_i(s_i | s_{i-1}, \dots, s_1)|^2 \right) \overbrace{\sum_{s_{k+1}} |\Psi_{k+1}(s_{k+1} | s_k, \dots, s_1)|^2}^{*=1} \\ &= \sum_{s_1, \dots, s_k} \tilde{\Psi}(s_1, \dots, s_k) \stackrel{**}{=} 1, \end{aligned}$$

where (\*) is because  $\Psi_{k+1}$  is a normalized conditional wave function, and (\*\*) because of the induction assumption.  $\square$

## Appendix B: Technical Details

In this section we cover the essential technical details of our models and how they are optimized.

### 1. Architecture

Our chosen architecture for our implementation of Neural Autoregressive Quantum State is loosely inspired by that of PixelCNN [18], which uses a row-wise ordering of the particles for the conditional wave-functions. All parameters and operations in the network are real, where the complex log-amplitudes of the conditional wave functions are represented as two real numbers, as discussed in the body. More specifically, it is composed of two interacting branches: (i) a “vertical” branch for representing

conditional dependencies between a given particle and all particles above it in the 2D lattice it resides on, and (ii) a “horizontal” branch for representing conditional dependencies between a given particle and all particles to its left. Each branch comprises a sequence of convolutional layers. The “vertical” containing convolutional layers with  $3 \times 3$  filters and 32 channels, where we add two rows of zero-padding to the top lattice before applying the convolution, to ensure a particle is not dependent on rows below it. For the “horizontal” branch, we use convolutional layers with  $3 \times 3$  filters and 32 channels, where we add two rows and two columns of zero-padding to the top and left of the lattice before applying the convolution, as well as setting the parameters at the (3,3) indices to be zero, all to ensure that a particle only depends on particles not “ahead” of itself according to the row-wise ordering we enforce. To combined them, the two branches are connected using the following scheme: after every convolutional layer in the “vertical” branch, but before the convolutional layer of the “horizontal” branch, we take the intermediate result of the “vertical” branch, shift every entry “down” along the vertical axis of the lattice, and concatenate it along the channels axis of the horizontal branch. The final convolutional layer of the “horizontal” branch serves as the output of the network, and hence we only use 2 output channels in that final layer, the two coordinates serving as the real and imaginary parts of the log-amplitude of the conditional wave-functions. The complete network can be depicted as a sequence of blocks, each as illustrated in fig. 4. We typically use between 10 and 40 such blocks, depending on the specific experiment. This separation of “vertical” and “horizontal” branches is a technique to overcome what is known as the “blind spot” problem of the original Pixel-CNN architecture (see van den Oord *et al.* [18] for more details).

## 2. Handling Symmetries

While our general NAQS architecture can already represent wave-functions quite well, we have found that leveraging the inherent symmetries of a given problem, e.g., invariance to rotations and flips, can dramatically improve the accuracy of our model. Specifically, we use a self-ensemble scheme to *symmetrize* our model, where for a model  $f(\mathbf{s})$  and a given input spin-configuration, we transform it according to its symmetries, denoted by the set  $\mathcal{T}$ , run each of them through our model, and aggregate the resulting log-amplitude outputs using the following equations for our symmetrize model  $\text{Sym}(f)$ :

$$\text{Re}(\text{Sym}(f)(\mathbf{s})) = \frac{1}{2} \ln \left( \sum_{T \in \mathcal{T}} \frac{1}{|\mathcal{T}|} e^{2 \cdot \text{Re}(f(T\mathbf{s}))} \right), \quad (\text{B1})$$

$$\text{Im}(\text{Sym}(f)(\mathbf{s})) = \text{Im} \left( \ln \left( \sum_{T \in \mathcal{T}} e^{i \cdot \text{Im}(f(T\mathbf{s}))} \right) \right). \quad (\text{B2})$$

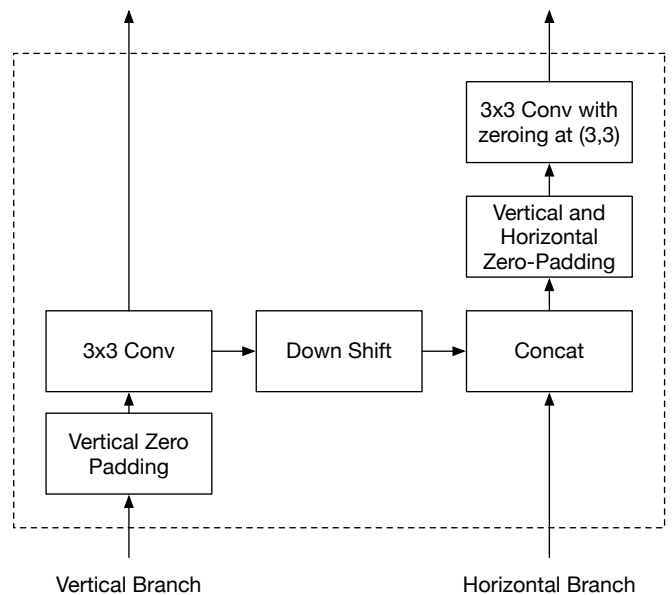


FIG. 4. An illustration of a single block that our architecture is composed of.

It is important to emphasize that while there are many ways to symmetrize a model, we cannot use any aggregation operation – it must also preserve its probabilistic meaning for we to be able to sample from it efficiently. We propose to incorporate the possible symmetries into our generative model, assuming we first sample a transformation  $T$  from  $\mathcal{T}$  with equal probability  $1/|\mathcal{T}|$ , and then draw a sample from our model as described in the main text, followed by transforming it with  $T$ . This translates to a mixture model over the squared magnitudes of the network’s predicted amplitude, and eq. B1 realizes it in log-space, where the real part of the output represent the log-magnitude. For the imaginary part, we have less restrictions and most symmetric operators would work, but we found that the *mean of circular quantities* of the phases, as expressed in eq. B2, worked best in our experiments.

## 3. Optimization

In our experiments we employ the following general optimization strategy. We begin using the Adam [23] SGD variant, using a small batch of 100 samples for estimating the gradient and using a learning rate in the order of  $10^{-3}$ . After about 10K gradient update steps, we increase the batch size to 1000, using the same learning rate and optimizer as the first stage, for an additional 10K update steps. In the final stage of the optimization, we increase the batch size again, and also switch to standard SGD with a momentum term, for an additional 5K update steps. For each experiment, we test multiple variations around the above default values of batch size,

learning rate, and number of update steps in each stage, and report the results for the best performing models.

- [1] W. L. McMillan, “Ground State of Liquid He4,” *Physical Review* **138**, A442–A451 (1965).
- [2] Robert Jastrow, “Many-Body Problem with Strong Forces,” *Physical Review* **98**, 1479–1484 (1955).
- [3] Mark Fannes, Bruno Nachtergaele, and Reinhard F Werner, “Finitely correlated states on quantum spin chains,” *Communications in mathematical physics* **144**, 443–490 (1992).
- [4] David Perez-García, Frank Verstraete, Michael M Wolf, and J Ignacio Cirac, “Matrix product state representations,” *Quantum Information and Computation* **7**, 401–430 (2007).
- [5] Frank Verstraete and J Ignacio Cirac, “Renormalization algorithms for quantum-many body systems in two and higher dimensions,” *arXiv preprint cond-mat/0407066* (2004).
- [6] Guifré Vidal, “Class of quantum many-body states that can be efficiently simulated,” *Physical review letters* **101**, 110501 (2008).
- [7] Giuseppe Carleo and Matthias Troyer, “Solving the quantum many-body problem with artificial neural networks,” *Science* **355**, 602–606 (2017).
- [8] Dong-Ling Deng, Xiaopeng Li, and S Das Sarma, “Quantum entanglement in neural network states,” *Physical Review X* **7**, 021021 (2017).
- [9] Jing Chen, Song Cheng, Haidong Xie, Lei Wang, and Tao Xiang, “Equivalence of restricted boltzmann machines and tensor network states,” *Phys. Rev. B* **97**, 085104 (2018).
- [10] Ivan Glasser, Nicola Pancotti, Moritz August, Ivan D. Rodriguez, and J. Ignacio Cirac, “Neural-network quantum states, string-bond states, and chiral topological states,” *Phys. Rev. X* **8**, 011006 (2018).
- [11] Raphael Kaubruegger, Lorenzo Pastori, and Jan Carl Budich, “Chiral topological phases from artificial neural networks,” *Physical Review B* **97**, 195136 (2018).
- [12] Hiroki Saito and Masaya Kato, “Machine Learning Technique to Find Quantum Many-Body Ground States of Bosons on a Lattice,” *Journal of the Physical Society of Japan* **87**, 014001 (2017).
- [13] Kenny Choo, Giuseppe Carleo, Nicolas Regnault, and Titus Neupert, “Symmetries and Many-Body Excitations with Neural-Network Quantum States,” *Physical Review Letters* **121**, 167204 (2018).
- [14] Yoav Levine, Or Sharir, Nadav Cohen, and Amnon Shashua, “Quantum entanglement in deep learning architectures,” *Physical review letters* (2019).
- [15] Benigno Uria, Marc-Alexandre Cote, Karol Gregor, Iain Murray, and Hugo Larochelle, “Neural Autoregressive Distribution Estimation,” *Journal of Machine Learning Research* () **17**, 1–37 (2016).
- [16] Dian Wu, Lei Wang, and Pan Zhang, “Solving Statistical Mechanics using Variational Autoregressive Networks,” (2018).
- [17] Juan Carrasquilla, Giacomo Torlai, Roger G Melko, and Leandro Aolita, “Reconstructing quantum states with generative models,” *Nature Machine Intelligence* **1**, 155–161 (2019).
- [18] Aaron van den Oord, Nal Kalchbrenner, Lasse Espeholt, Oriol Vinyals, Alex Graves, *et al.*, “Conditional image generation with pixelcnn decoders,” in *Advances in Neural Information Processing Systems* (2016) pp. 4790–4798.
- [19] Prajit Ramachandran, Tom Le Paine, Pooya Khorrami, Mohammad Babaeizadeh, Shiyu Chang, Yang Zhang, Mark A Hasegawa-Johnson, Roy H Campbell, and Thomas S Huang, “Fast generation for convolutional autoregressive models,” *arXiv preprint arXiv:1704.06001* (2017).
- [20] Giacomo Torlai, Guglielmo Mazzola, Juan Carrasquilla, Matthias Troyer, Roger Melko, and Giuseppe Carleo, “Neural-network quantum state tomography,” *Nature Physics* **14**, 447 (2018).
- [21] Bjarni Jnsson, Bela Bauer, and Giuseppe Carleo, “Neural-network states for the classical simulation of quantum computing,” *arXiv:1808.05232 [cond-mat, physics:physics, physics:quant-ph]* (2018), *arXiv*: 1808.05232.
- [22] Henk W. J. Blte and Youjin Deng, “Cluster Monte Carlo simulation of the transverse Ising model,” *Physical Review E* **66** (2002), 10.1103/PhysRevE.66.066110.
- [23] Diederik Kingma and Jimmy Ba, “Adam: A method for stochastic optimization,” 3rd International Conference on Learning Representations (ICLR) (2014).
- [24] Wen-Yuan Liu, Shao-Jun Dong, Yong-Jian Han, Guang-Can Guo, and Lixin He, “Gradient optimization of finite projected entangled pair states,” *Physical Review B* **95**, 195154 (2017).
- [25] Giuseppe Carleo and Matthias Troyer, “Solving the quantum many-body problem with artificial neural networks,” *Science* **355**, 602–606 (2017).
- [26] Kenny Choo, Titus Neupert, and Giuseppe Carleo, “Study of the two-dimensional frustrated j1-j2 model with neural network quantum states,” *arXiv preprint arXiv:1903.06713* (2019).
- [27] B. Bauer, L. D. Carr, H. G. Evertz, A. Feiguin, J. Freire, S. Fuchs, L. Gamper, J. Gukelberger, E. Gull, S. Guertler, A. Hehn, R. Igarashi, S. V. Isakov, D. Koop, P. N. Ma, P. Mates, H. Matsuo, O. Parcollet, G. Pawowski, J. D. Picon, L. Pollet, E. Santos, V. W. Scarola, U. Schollwck, C. Silva, B. Surer, S. Todo, S. Trebst, M. Troyer, M. L. Wall, P. Werner, and S. Wessel, “The ALPS project release 2.0: open source software for strongly correlated systems,” *Journal of Statistical Mechanics: Theory and Experiment* **2011**, P05001 (2011).